PHYSICAL REVIEW B **81**, 085324 (2010)

First-principles density functional study of dopant elements at grain boundaries in ZnO

Wolfgang Körner* and Christian Elsässer
Fraunhofer Institute for Mechanics of Materials IWM, Wöhlerstr. 11, 79108 Freiburg, Germany
(Received 11 November 2009; revised manuscript received 18 January 2010; published 18 February 2010)

We present a first-principles density functional theory study of doped ZnO with focus on its application as a transparent conducting oxide, having both high optical transparency and high electrical conductivity. Investigated is the impact of grain boundaries on the physics of atomic defects, and especially the formation energies of oxygen vacancies, cation dopants Al and Ga, and anion dopants N and P are determined. The main goal is to obtain information about the positions of the defect levels generated by the different dopants in the electronic band gap. Because of the known deficiency of the local density approximation (LDA) to yield accurate values for band gap energies for insulators such as ZnO a self-interaction correction (SIC) to the LDA is employed. As atomistic supercell models which contain grain boundaries and dopants are quite large in size we implemented the SIC by means of SIC pseudopotentials which merely increase the computational costs, as compared to the LDA. The main result of our study is that grain boundaries do affect the formation energies for substitutional dopants significantly. Furthermore the position and shape of dopant-induced electronic energy levels at the grain boundaries are changed considerably with respect to the single crystal. This may help us to explain, for example, why N doping can lead to *p* conductivity at room temperature or why Al or Ga doping can increase the transparency.

DOI: 10.1103/PhysRevB.81.085324 PACS number(s): 61.72.Bb, 61.72.Mm, 71.55.Gs

I. INTRODUCTION

Transparent conducting oxide (TCO) thin film systems are getting widely used as electrodes in photovoltaic and optoelectronic technologies. Mainly doped oxidic semiconductors are applied which have simultaneously a high electrical conductivity and a high optical transmission in the visible spectral range. Most TCO materials available today do not yet fulfill both requirements satisfactorily. The best material at present is indium tin oxide (ITO). However, the price of indium has increased tenfold since the year 2002, which already impedes the introduction of ITO-based products to the market and promotes the search for other TCO materials.

A promising alternative TCO is ZnO which has been subject to intensive research in recent years. Numerous first-principles density functional theory (DFT) studies investigated different aspects of the physics of atomic defects and dopants. Various kinds of model systems were evaluated, e.g., intrinsic atomic defects in ZnO,[1–5] *n* doping of ZnO with Al or F,[4] *p* doping of ZnO with N, P, As, Sb, Li, Na, K, Cu, Ag, or Au,[6–11] or *p* codoping with N and Ga.[12,13] All these DFT studies dealt with the single crystal of ZnO, having the hexagonal wurtzite structure, as a basic host material model for point-defect supercell calculations. However, real ZnO materials are usually polycrystalline with typical grain sizes of 30–100 nm.[14] This implies that ZnO systems contain many grain boundaries (GBs) which can influence the point-defect physics. Not only the formation energies for certain point defects may change in the vicinity of a grain boundary but also defect levels in the electronic band structure may be altered. All these motivate an investigation of the influence of different dopant elements at grain boundaries and their capability to achieve satisfactory *n* or *p* conductivity of the polycrystalline TCO material.

The importance of grain boundaries in ceramics has stimulated a large number of DFT studies, e.g., Refs. 15–30. In order to come to a realistic and reliable atomistic model for our study of doped polycrystalline ZnO we constructed a set of three supercell models that have atomic structures of experimentally observed grain boundaries in ZnO bicrystals.[14,31,32] By first-principles DFT calculations we compare these grain boundaries with the bulk single crystal in order to analyze the influence of the grain boundaries on the formation energies and the electronic structures of the point defects. We have chosen a set of dopant elements with regard to TCO applications. N and P are candidates for *p* doping that have so far only been investigated in the bulk single crystal. For *n* doping we have chosen Al and Ga. As important intrinsic point defect we investigated the oxygen vacancy which is seen as a key reason for the intrinsic *n* conductivity of undoped ZnO.

Previous DFT studies have found that undoped grain boundaries in ZnO (Refs. 33–35) do not create deep defect states in the band gap whether they are stoichiometric or not. To our knowledge only one group so far studied the combination of a grain boundary ($\Sigma 13, 32, 3°[0001]$) and dopants (Sn, Bi) in ZnO in the context of varistors.[36–40] For their dopants the calculations reveal a strong tendency of segregation to the boundary. Furthermore their results indicate that native defects and impurities do not create electrically active grain boundaries. Interfacial complexes however can lead to deep acceptor states resulting in grain boundaries with *p*-type character.

The study is guided by three principal questions: (1) Which substitutional sites in ZnO are occupied by the dopants? (2) How large are the defect-formation energies for the dopants? (3) Which electronic defect levels do the dopants create? In order to answer the first two questions we determine the formation energies of the different substitutional dopants in the single crystal and at the grain boundaries. This delivers information about the segregation behavior and how easy a certain dopant can be incorporated. The answer to the third question, a detailed knowledge of electronic levels, pro-

 ©2010 The American Physical Society

vides information about the electrical and optical properties of the doped ZnO. As TCO require both high optical transparency and electrical conductivity (delocalized) defect states near the band edges would be desirable.

In order to address the questions above one needs an extension of the local density approximation (LDA) [or the generalized gradient approximation (GGA) as well]. Unfortunately in the case of II-VI semiconductors, namely, ZnO, the LDA has certain known shortcomings. The d bands have been found in several LDA calculations[41–45] to occur about 3 eV too high in energy as compared to photoelectron experiments,[46–50] falsifying also the dispersion and bandwidth of the valence band formed by anion p states. Furthermore the band gap is underestimated by more than 50%.[41,45] From the work of Perdew and Zunger[51] on free atoms it is known that these insufficiencies originate from the unphysical self-interaction that is present in approximate exchange-correlation functionals (LDA or GGA) of DFT. The self-interaction is most pronounced for tightly bound and highly localized states (e.g., $3d$ of Zn or $2p$ of O). Thus these states have significantly misplaced energy levels.

There are several DFT schemes, e.g., LDA+U, self-interaction correction (SIC)-LDA, or GW, which are capable to improve certain LDA results. In our investigation we deal with large grain-boundary supercells of up to 152 atoms which demand a computation scheme that is not more involved than the LDA. We have adapted a SIC scheme that is close to the one described by Vogel *et al.*[52] where the SIC is incorporated in norm-conserving pseudopotentials (PPs) that represent the core-valence interactions. Vogel *et al.*[52] gave a clear review of the development of the SIC and explained in detail how the SIC can be implemented into the PP approach.

Our paper is organized as follows. In Sec. II A we give the computational details about our LDA calculations. In Sec. II B our implementation of the SIC is described. In Sec. II C we explain our supercell models. The obtained results of the total-energy calculations are presented in Sec. III. The electronic-structure results are in Sec. IV. A concise summary in Sec. V concludes the paper.

II. THEORETICAL APPROACH

A. Mixed-basis pseudopotential method

The total-energy and electronic-structure calculations in this work were carried out on the basis of DFT by means of the computational mixed-basis pseudopotential (MBPP) method.[53–57] We used the LDA for exchange-correlation from Ceperley and Alder[58] as parametrized by Perdew and Zunger.[51] For Zn, O, and the impurity elements (Al, Ga, N, and P) norm-conserving pseudopotentials[59] were used for the core-valence interactions. The valence Bloch states were represented by a mixed basis of plane waves and additional nonoverlapping atom-centered p orbitals for O and N ($2p$ states) and d orbitals for Zn and Ga ($3d$ states). A plane-wave cutoff energy of 20 Ry was determined to be sufficient for getting well converged results. For the k-point sampling of the Brillouin-zone integrals in the total-energy calculations the Monkhorst-Pack scheme and a Gaussian broadening of 0.2 eV were used. For more information on the MBPP method used for doped grain boundaries in metal oxides see, e.g., Ref. 29.

For the determination of defect-formation energies in semiconductors the application of the LDA is not sufficient, as shown, for example, by Lany and Zunger.[60] Our correction scheme for the band gap error which uses the SIC follows their strategy (see the Appendix of Ref. 61 for a detailed explanation). Also for the investigation of positions of the additional energy levels due to dopants in the electronic band structure one needs to go beyond LDA.

B. Self-interaction corrected pseudopotentials

As mentioned in Sec. I we have chosen an implementation of the SIC that does not increase considerably the computational effort and thus is applicable to large atomistic supercells with up to 152 atoms. Initially we closely follow the work of Vogel *et al.*[52] who incorporated the SIC into pseudopotentials for the atoms involved. The SIC-LDA calculations for supercells are then performed as the usual LDA calculations unless now the SIC-LDA PPs are used instead of LDA PP. A detailed description of this approach has been given by Vogel *et al.*[52] In the following we summarize it concisely and indicate a few practical modifications.

We start by solving the one-particle all-electron Kohn-Sham equations in LDA for free atoms of the involved elements,

$$\left(-\nabla^2 - \frac{2Z}{r} + V_{\mathrm{H}}[n] + V_{\mathrm{xc}}[n]\right)\Psi_i = \epsilon_i \Psi_i, \tag{1}$$

where $n=\Sigma_i n_i$ is the total electron charge density (in atomic Rydberg units). V_{H} and V_{xc} are the electrostatic Hartree and LDA exchange-correlation potentials and Ψ_i and ϵ_i are the one-electron orbital wave functions and energy eigenvalues. The electron density of an orbital i is given by $n_i=p_i|\Psi_i|^2$, where p_i is the orbital occupation number. Then we construct norm-conserving ionic PP $V_{n,l}(r)$ for the valence electrons (for instance, by the scheme proposed by Vanderbilt[59]). The subscripts n and l denote the principal and angular-momentum quantum numbers of the respective highest valence orbital. In the case of zinc (oxygen), for example, we create such PP for the $3d$, $4s$, and $4p$ ($2s$, $2p$, and $3d$) orbitals. In the following we omit the quantum number n since it is unique and only write V_l. As next step we solve by iteration

$$(-\nabla^2 + V_l + V_{\mathrm{H}}[n_v] + V_{\mathrm{xc}}[n_v] \underbrace{- w_l[V_{\mathrm{H}}[n_l] + V_{\mathrm{xc}}[n_l]]}_{:=-V_{\mathrm{cor}}[n_l]})\Psi_l^{pp} = \epsilon_l^{pp}\Psi_l^{pp}, \tag{2}$$

where n_v is the pseudodensity of all valence electrons $n_v=\Sigma_l n_l$ and $n_l=p_l|\Psi_l^{pp}|^2$ is the pseudodensity of electron orbital l. Weight factors w_l are introduced which can take values in between 0 and 1. With all $w_l=1$ Eq. (5) of Ref. 52 is obtained. They call this correction scheme *atomic* SIC (ASIC) as they apply the SIC to isolated atoms taking the atomic occupations. The weight factors allow us to turn on and off the SIC gradually. The advantage is that one can build PPs that are better adjusted to the local environment in

a solid. In the ionic compound ZnO, for example, the 4*s* and 4*p* orbitals of Zn are nearly unoccupied. We take this into account by setting $w_0=0$ and $w_1=0$, which means we do not apply the SIC to the 4*s* and 4*p* orbitals of Zn. For the 3*d* orbitals we choose $w_2=1$ as they are almost fully occupied in ZnO and thus need to be maximally corrected as in the free Zn atom.

Vogel *et al.*[52] defined the SIC PP as $V_l^{\mathrm{SIC}} := V_l - V_{\mathrm{H}}[n_l] - V_{\mathrm{xc}}[n_l]$. These SIC pseudopotentials however cannot be transferred directly from the atoms to the solid because they have asymptotic $-2/r$ tails from the Coulomb potential $V_{\mathrm{H}}[n_l]$. Such long-range potentials would cause an ill convergent overlap of SIC contributions at different atoms in the solid. Fortunately it is the product $V_{\mathrm{Coul}}[n_l]\Psi_l^{pp}$ that appears in Eq. (2), which is of short range because the wave functions are localized, and hence the PP overlap is avoidable. For the zinc and oxygen atoms Vogel *et al.* showed the radial dependence of these wave functions and the corresponding corrections in Fig. 3 of Ref. 52. With the above mentioned argument they shifted the SIC PP V_l^{SIC} in energy and set it equal to zero outside a radius of about 8 a.u. Apart from being still quite extended these SIC PPs have a discontinuity in real space which causes long-range oscillations in Fourier-space representations of the PP. Therefore we have chosen a different implementation of the SIC PP for our MBPP code, which uses a mixed representation in real and Fourier spaces. We project the self-interaction correction term $V_{\mathrm{cor}}[n_l]$ of Eq. (2) onto the valence wave functions Ψ_l^{pp} to obtain a Kleinman-Bylander-type operator form of the SIC PP,

$$V_l^{\mathrm{SIC}}(r) := V_l(r) - \alpha\langle\Psi_l^{pp}, V_{\mathrm{cor}}[n_l]\Psi_l^{pp}\rangle\Psi_l^{pp}(r), \quad (3)$$

where $\langle\cdots,\cdots\rangle$ denotes the scalar product. Additionally we introduce a factor α at this point, as Filippetti and Spaldin[62] who use a value of 0.5 for α, in order to mimic relaxation effects of the electrons in the solid. This choice is not justified in general. Pemmaraju *et al.*[63] allowed α to vary as an empirical parameter and interpreted it as a measure of the deviation of the ASIC potential from the exact SIC potential of the solid. They showed that α is close to 1 for systems which have atomiclike charge density and it reduces to 0.44 for medium- to wide-gap semiconductor compounds.

Putting the explicit expression of $V_{\mathrm{cor}}[n_l]$ into Eq. (3) one can see that the weight factors w_l and the parameter α could be merged. The advantage would be to have less parameters in the model. However, we prefer to keep the parameters separated as they can be connected to physical properties of the considered system. As already mentioned, the w_l is closely linked to the orbital occupation[52] and the α can be interpreted as a solid-state adjustment of the atomic SIC.[63] The values the parameters taken in our model of ZnO are listed in Table I and explained in detail in Secs. II A and II B.

C. Supercells for grain boundaries

For ZnO impressive experimental atomic-scale images of grain boundaries were obtained by Oba *et al.*[14] and Sato and Yamamoto[31] by high-resolution transmission electron microscopy of high-quality ZnO bicrystals. Arbitrarily misoriented GBs (i.e., general GB with high values of the coincidence site lattice (CSL) parameter Σ) are problematic for first-principles studies because of large periodicity lengths parallel to the interface plane. Furthermore in order to suppress GB-GB interactions in supercells with three-dimensional periodic boundary conditions a sufficient number of layers of bulk structure in between two adjacent grain boundaries are needed. This requirement excludes most experimentally observed grain boundaries since these would require huge supercells with computationally untractable number of atoms. Inspired by Oba *et al.*[14] and Sato and Yamamoto[31] we have selected a representative set of three suitable grain boundaries with distinct structural units at the boundary plane. These supercell models are displayed in Figs. 1–3 and specified in Table II in terms of their boundary plane, the tilt axis, CSL parameter Σ, the numbers of atoms per supercell, and the GB energy obtained by LDA calculations (see below).

Next, the supercell models of the single crystal and the grain boundaries containing dopants were constructed. We substituted either an oxygen atom by nitrogen or phosphorus or a zinc atom by aluminum or gallium. Although there exist many more defect configurations, such as interstitials or complexes of substitutional impurities with oxygen or zinc vacancies, this study is restricted to single-atom substitution for now in order to get scientific insight into the increased structural and electronic complexities of ZnO containing both dopants and boundaries with reasonable research effort. Additionally, the oxygen vacancy as one important intrinsic point defect was investigated for comparison. Furthermore different charge states of the defects were considered by relaxing the GB structures with different numbers of electrons exchanged between Bloch states and a homogeneous jellium background, ensuring that the charge neutrality of the supercells is conserved.

TABLE I. Table of the weight factors w_l introduced in Eq. (2). The values given above were used for the SIC-LDA calculations in this study.

Weight factor	Zn	O	N	P	Al	Ga
w_0	0	1.0	1.0	1.0	0	0
w_1	0	0.8	0.8	0.8	0	0
w_2	1.0	0	0	0	0	1.0

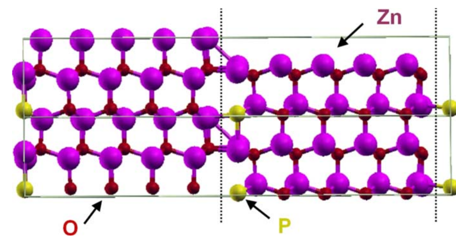

FIG. 1. (Color online) View from $[1\bar{2}10]$ on two supercells (box of solid lines) of the GB1: $(10\bar{1}0)[10\bar{1}0]$ $\Sigma 1$ doped with P substituting O at the boundary. The dotted lines indicate the grain boundaries.

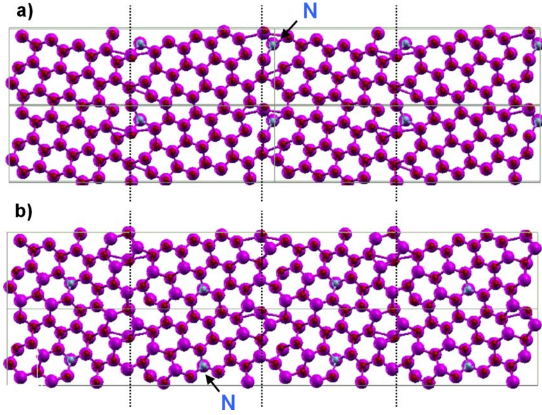

FIG. 2. (Color online) View from [0001] on four supercells (112 atoms each) of the GB2:$(12\bar{3}0)[0001]$ $\Sigma 7$ doped with N substituting O (a) at the GB and (b) in the bulk region. The dotted vertical lines indicate the grain boundaries. Note that along the [0001] direction the atomic columns consist of alternating Zn and O atoms.

Due to the periodic boundary conditions every supercell contains two equivalent grain boundaries. Thus, for example, two oxygen atoms are substituted by two phosphorus atoms like in Fig. 1 in order to preserve equivalence of the two boundaries. For the different boundaries we always only replaced each two host atoms per supercell, which resulted in doping concentrations of 2.5% for the $(10\bar{1}0)[10\bar{1}0]$ $\Sigma 1$, 1.8% for the $(12\bar{3}0)[0001]$ $\Sigma 7$, and 1.3% for the $(23\bar{5}0)[0001]$ $\Sigma 19$ supercell. As reference bulk structure we used a hexagonal $3 \times 3 \times 2$ supercell of 72 atoms (36 formation units) where the substitution of one zinc or oxygen atom corresponds to a impurity concentration of 1.4%.

III. TOTAL-ENERGY RESULTS AND DISCUSSION

A. ZnO single crystal

As a prerequisite for the study of dopants and interfaces, the three structural parameters of the ZnO single crystal in the wurtzite structure were determined by DFT calculations with the MBPP code and LDA-PP. The values $a=3.227$ Å, $c/a=1.6$, and $u=0.38$ were obtained that underestimate the experimental values[64] $a=3.258$ Å, $c/a=1.6022$, and $u=0.382$ by less than 1%, which are typical deviations for LDA results.

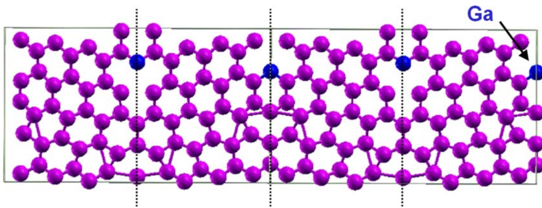

FIG. 3. (Color online) View from [0001] on two supercells of the GB3:$(23\bar{5}0)[0001]$ $\Sigma 19$ where Ga atoms substitute Zn atoms in the boundary region. The dotted lines indicate the grain boundaries. Note that along the [0001] direction the atomic columns consist of alternating Zn and O atoms.

TABLE II. Supercell models for grain boundaries in wurtzite ZnO. The boundary energy is the energy needed to insert the grain boundary into the bulk single crystal. In the text the three grain boundaries are denoted by GB1, GB2, and GB3.

Grain boundary notation	Atoms per supercell	GB energy (J/m^2)
GB1:$(10\bar{1}0)[10\bar{1}0]$ $\Sigma 1$	80	0.17
GB2:$(12\bar{3}0)[0001]$ $\Sigma 7$	112	1.89
GB3:$(23\bar{5}0)[0001]$ $\Sigma 19$	152	1.65

B. ZnO grain boundaries

The three grain-boundary models studied in this work are listed in Table II and displayed in Figs. 1–3. Their supercells were structurally relaxed by the shifting the atoms according to the Broyden-Fletcher-Goldfarb-Shanno (BFGS) algorithm[65] until the residual forces on all atoms were below 0.001 Ry/a.u. (atomic units: 1 Ry=13.606 eV, 1 a.u. =0.529 Å). From the differences of total energies of the undoped boundary supercells and the corresponding bulk supercells we determined the GB energies. The $(10\bar{1}0)[10\bar{1}0]$ $\Sigma 1$ GB shown in Fig. 1 (abbreviated as GB1 in the following) is only a weak disturbance of the perfect wurtzite structure. The two other grain boundaries, $(12\bar{3}0)[0001]$ $\Sigma 7$ (GB2) and $(23\bar{5}0)[0001]$ $\Sigma 19$ (GB3), which are shown in Figs. 2 and 3, deviate more from the perfect crystal and require more energy to be formed.

In Table II the energies of the three considered GBs are listed. As already mentioned, GB1 is only a weak disturbance of the bulk single crystal which is reflected in its low energy of only 0.17 J/m^2. There have been previous atomic simulations by Oba *et al.*[35] for the $(12\bar{3}0)[0001]$ $\Sigma 7$. Their boundary A in Ref. 35 with a GB energy of 1.45 J/m^2 determined with LDA corresponds to our GB2 with 1.89 J/m^2. The difference in the GB energy is probably due to the different supercell sizes (80 atoms vs 112 atoms) or other computational settings (pseudopotentials, basis sets, *k*-point meshes, etc.).

C. Formation and segregation energies

For the supercell models of the ZnO grain boundaries described in Sec. III B we determined the defect-formation and boundary-segregation energies of the different doping elements. For the calculation of the formation energies we applied the thermodynamic formalism which is extensively explained, for instance, in the review of Van de Walle and Neugebauer.[66] The defect-formation energy of a dopant atom at a grain boundary (m=GB) or in the bulk interior (m=bulk) is determined by

$$E_{\mathrm{f}}^{\mathrm{m}}(d,q) = E_{\mathrm{tot}}^{\mathrm{m}}(d,q) - E_{\mathrm{tot}}^{\mathrm{m}}(h,q=0) + \mu(h) - \mu(d) - q\mu_e, \tag{4}$$

where $E_{\mathrm{tot}}^{\mathrm{m}}(d,q)$ is the total energy of the supercell containing the defect d [d=N, P, Al, Ga, or O_{vac}(=oxygen vacancy)]

TABLE III. Segregation energies of the four considered dopants (values in eV) for the three different grain boundaries as determined by the two methods described. The results obtained by method 2 are given in brackets.

GB	$E_{seg}(N_O)$	$E_{seg}(P_O)$	$E_{seg}(Al_{Zn})$	$E_{seg}(Ga_{Zn})$
GB1	0.05 (0.05)	0.11 (0.06)	0.01 (0.04)	0.09 (0.05)
GB2	−1.47 (−0.22)	−2.61 (−1.49)	−1.42 (−0.05)	−1.16 (0.08)
GB3	0.06 (0.04)	−1.60 (−1.93)	−0.20 (0.67)	−0.61 (−0.02)

plus q excess electrons. $E_{tot}^{m}(h,q=0)$ is the total energy of the uncharged grain boundary or bulk supercell where the host atom h (h=O or Zn) is not substituted. $\mu(h)$ and $\mu(d)$ denote the chemical potentials of the host and dopant atoms. μ_e is the chemical potential of the electrons (the Fermi level) relative to the valence-band maximum, ranging from 0 to 3.4 eV in the energy gap between the valence and conduction band edges in the case of ZnO.

The value of the defect-formation energy for a certain dopant element strongly depends on the reference material. Yan *et al.*[67] discussed N doping of ZnO with the four source gases N_2, NO, NO_2, and N_2O as references. They showed how the formation energy of N substituting O varied with the choice of the source gas. Since the choice of the source is not unique we have selected stable materials that are likely to appear in growth processes. As reference that compete with the incorporation in the crystal we have chosen gaseous molecular O_2 for oxygen and N_2 for nitrogen. For the other doping materials we have taken oxidic solid-state compounds. As reference materials for phosphorus we have taken P_4O_{10} and for the metals aluminum and gallium we have chosen Al_2O_3 and Ga_2O_3.

In order to determine the grain-boundary-segregation energy E_{seg} we used two methods. Method 1, applied for example by Carlsson *et al.* to doped GB in ZnO,[39] is to calculate the formation energy of the defect in the grain-boundary supercell and in the corresponding single crystal supercell of same size. Then $E_{seg}=E_f^{GB}(d,q)-E_f^{bulk}(d,q)$. For method 2, often used for doped GB in metals (cf. Ref. 29 for oxides), one has to calculate as well the total energy of the grain-boundary supercell with the dopant sitting in the bulk region between and as far as possible away from the interfaces which appear periodically. Such a supercell arrangement is depicted in Figs. 2(a) and 2(b) for N incorporated in a GB2 supercell. The segregation energy is then the difference of the total energies of the supercells with the impurity at the boundary E_{tot}^{GB} and in the bulk region E_{tot}^{BR}: $E_{seg}=E_{tot}^{GB}(d,q)-E_{tot}^{BR}(d,q)$. Negative values of the segregation energy indicate the tendency of the dopant to prefer a site at the boundary. Our results obtained with method 1 (and method 2) for the four dopant species at the three grain boundaries are given in Table III.

Looking at the values of method 1 one can see a tendency for the dopants to segregate to the GB2 and GB3 (except N for GB3). The segregation energies for GB1 are slightly positive but can be estimated as being almost zero. This is understandable as the atomic structure of GB1 is very similar to that of the bulk crystal.

TABLE IV. Comparison of the defect-formation energies of the uncharged dopants (charge state $q=0$) for the three different grain boundaries under oxygen-rich conditions $\mu_O=0$ eV. All dopants show a lower formation energy at GB2 than in the bulk crystal whereas the incorporation at GB1 or GB3 costs partially even more energy (see Al in GB3 for example).

Formation energies (eV)	N_O	P_O	Al_{Zn}	Ga_{Zn}
E_f^{bulk}	1.75	17.16	4.06	3.18
E_f^{GB1}	1.82	17.11	4.43	3.62
E_f^{GB2}	0.85	14.21	2.67	2.19
E_f^{GB3}	1.76	13.09	4.54	2.91

From method 2 segregation-energy values are obtained which are close to zero except for the case of phosphorus. We conclude from this finding that the electronic screening in the GB supercells is too weak, implying that the boundaries are too close to atoms sitting in the bulk regions of the supercells. In the case of GB2 for example (Fig. 2) the N atom is only separated by two bulk ZnO layers from the GB. In systems with more efficient screening (like metallic conductors) or much larger supercells the results obtained by methods 1 and 2 should be equal. Unfortunately a stringent convergence check for ZnO GB by increasing the supercell sizes is not feasible with the available resources.

In summary, we deduce a trend of segregation to the GB for phosphorous that is conceivable due to size mismatch of P and O. The other dopants resemble more to their substituted host atoms and thus do not show a clear tendency of segregation.

In Table IV the formation energies of the neutral defects in the bulk region and at the different GBs are listed. Comparing the formation energies of a certain dopant at the three different boundaries and in the bulk crystal, one notices variations of several eV. For phosphorous one can extract the trend of lower formation energies at boundary positions, which is also reflected by the negative segregation energies in Table III. For the other dopants a rather mixed picture emerges. At GB1 the formation energies are partly higher than in the bulk crystal. Due to the periodic restriction of the supercell in all three dimensions one simulates an array of impurities. Since the supercell sizes of GB1 and the bulk are different one is comparing different concentrations of impurities. We conclude that a high dopant concentration of N, Al, or Ga at GB1 is less favorable than a dilute dopant distribution in the bulk region. At GB2 N, Al, and Ga show lower formation energies than in the bulk whereas the formation energies at GB3 are equal or higher than in the bulk. Analyzing the relaxed atomic structures of GB2 and GB3 one notices bond lengths that differ by about 10% from the bulk values, indicating strong relaxations at both GBs. A difference between GB2 and GB3 is obtained concerning the coordination number of the dopants. It is four at GB2 and three at GB3. We conclude that having four nearest neighbors like in the bulk is energetically favorable.

In order to get a complete picture of the formation energies one also has to consider different charge states of the

TABLE V. Comparison of the defect-formation energies of the dopants in different charge states determined in a 72-atom bulk single crystal supercell and in the grain-boundary supercells GB1 and GB2 (only the preferred charge states that appear in Fig. 4 are listed). The energies are given in eV. The last column gives the dependence of the formation energy on the chemical potentials. The charge neutral defects N_O, P_O, Al_{Zn}, and Ga_{Zn} are given in Table IV. The chemical potentials μ_O and μ_e can vary in the intervals $H_F[ZnO] \leq \mu_O \leq 0$ eV (experimental enthalpy of formation value $H_F[ZnO]=-3.6$ eV (Ref. 68)) and $0 \leq \mu_e \leq E_g$ [experimental band gap value $E_g=3.4$ eV (Ref. 69)]. $\mu_O=0$ eV corresponds to O-rich conditions and $\mu_O=-3.6$ eV corresponds to Zn-rich conditions.

Defect	E_f^{bulk} (eV)	E_f^{GB1} (eV)	E_f^{GB2} (eV)	Dependency on μ_O and μ_e
O_{vac}	4.49	4.38	4.12	$+\mu_O$
O_{vac}^{2+}	2.39	2.99	2.67	$+\mu_O+2\mu_e$
N_O^-	5.86	6.30	6.24	$+\mu_O-\mu_e$
P_O^{2-}	21.44	20.94	19.08	$+\frac{7}{2}\mu_O-2\mu_e$
P_O^{3-}	24.15	22.38	21.83	$+\frac{7}{2}\mu_O-3\mu_e$
P_O^{2+}	12.17	10.57	10.24	$+\frac{7}{2}\mu_O+2\mu_e$
P_O^{3+}	11.78	10.01	9.95	$+\frac{7}{2}\mu_O+3\mu_e$
Al_{Zn}^+	0.01	0.26	−1.55	$+\frac{1}{2}\mu_O+\mu_e$
Ga_{Zn}^+	−0.76	−0.41	−1.67	$+\frac{1}{2}\mu_O+\mu_e$

impurities. In Table V the defect-formation energies in the bulk crystal and of the GB1 and GB2 are listed for the substitutional dopants in various charge states. Only those charge states which have the lowest formation energy in some range of the chemical potential within the band gap are listed. In the last column the dependence on the oxygen chemical potential μ_O and the electronic chemical potential μ_e is also given. In Figs. 4 and 5 the charge states of the impurities for the bulk single crystal and GB2 supercell as a function of the electronic chemical potential μ_e are displayed. (We omitted the figure for GB1 because it is very similar to Fig. 4.) Values of μ_e close to 0 eV correspond to the p-conduction regime whereas values of μ_e close to 3.4 eV correspond to the n-conduction regime.

Our results obtained for the oxygen vacancy are in good agreement with the results given by Lany and Zunger.[60] Especially our formation energy for the neutral defect $E_f^{bulk}(O_{vac})=4.49$ eV is close to their value of 4.67 eV.

From Figs. 4 and 5 the difficulty of p doping of ZnO can be made conceivable. Lowering of the Fermi level by p doping (with N or P) lowers the formation energy of the oxygen vacancy which in turn reduces the p conductivity. Comparing the dopant candidates for p conductivity N can be incorporated more easily into the ZnO crystal than P since its size deviates less from the size of an oxygen atom. [Our absolute values for $E_f^{bulk}(N_O)$ and $E_f^{bulk}(N_O^-)$ agree very well with the results obtained in Refs. 9 and 12.] Furthermore P is more strongly bound in P_4O_{10} than N in N_2. The enthalpies of formation are $\Delta H_f(P)=-27.58$ eV/atom and $\Delta H_f(N)=-8.36$ eV/atom (calculated with LDA). Notice that the formation energy of substitutional phosphorus is high but can be reduced considerably by going from O-rich to Zn-rich conditions [by $\frac{7}{2}(-3.6\text{ eV})=-12.6$ eV; see last column of Table V]. But still the formation energy remains high in comparison to substitutional nitrogen or the intrinsic oxygen vacancy. Furthermore phosphorous shows amphoteric behavior which means it works against the "desired" regime. In the p-conduction regime phosphorous acts as a donor (P_O^{3+}-defect state) and in the n-conduction regime as an acceptor (P_O^{3-}-defect state), and thus it reduces the amount of free charge carriers.

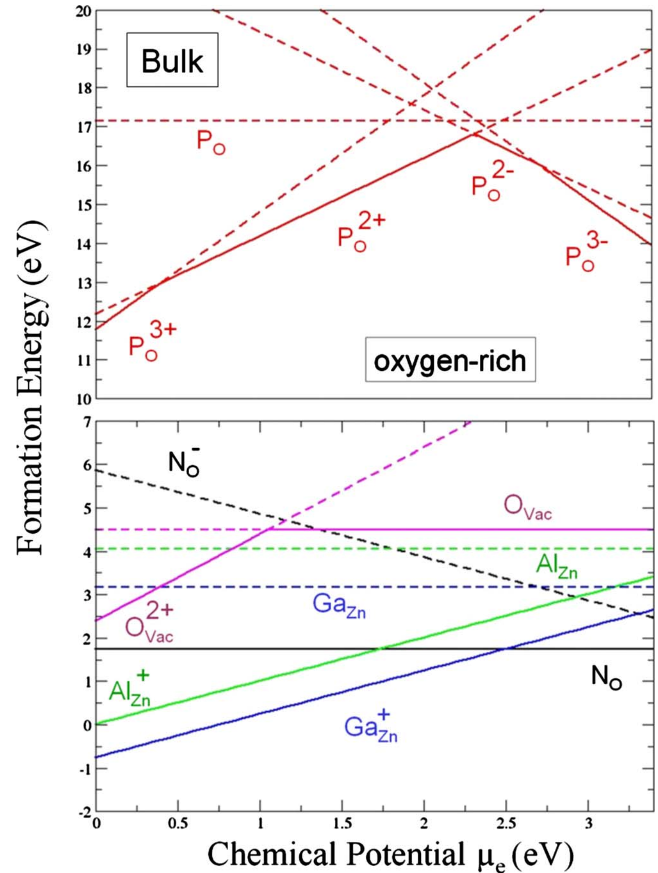

FIG. 4. (Color online) Defect formation energies for the dopants in the bulk single crystal as a function the chemical potential μ_e of the electrons under oxygen-rich conditions ($\mu_O=0$) (unfavorable charge states are plotted with dashed lines). Values of μ_e close to 0 eV correspond to the p-conducting regime, whereas values of μ_e close to 3.4 eV correspond to the n-conducting regime. Lowering the chemical potential by p doping lowers the formation energy of the oxygen vacancy (O_{vac}) which in turn reduces the p conductivity. For the GB1 supercell very similar results were obtained in the sense that the same charge states were preferred (see Table V). The results are mainly shifted upward or downward in energy. The results for the GB2 supercell which also only differ for phosphor are shown in Fig. 5.

Looking at Al and Ga, the dopant candidates for n conductivity, we notice that the positively charged defect states Al_{Zn}^+ and Ga_{Zn}^+ are lower in energy than the charge neutral states. Lany and Zunger[70] reported the same behavior for the Al defect except for a small range of μ_e at the conduction band minimum (CBM). In general, Ga has a lower formation energy than Al. This is conceivable because first the atomic size of the gallium atom is closer to the one of zinc.

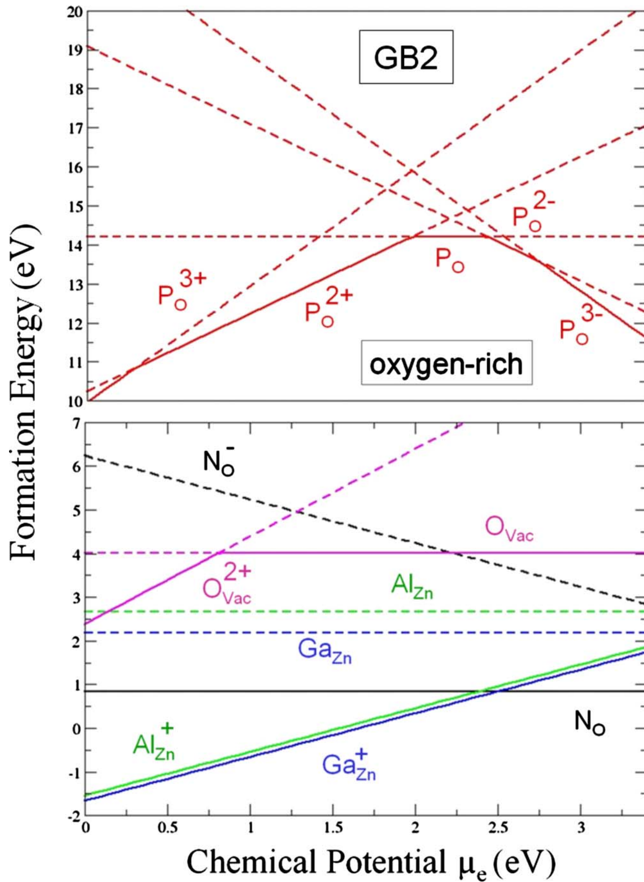

FIG. 5. (Color online) Defect formation energies for the dopants at GB2 as a function of the chemical potential μ_e of the electrons under oxygen-rich conditions ($\mu_O=0$) (unfavorable charge states are plotted with dashed lines). The GB2 supercell results were obtained in the sense that the same charge states were preferred (see Table V).

Thus less deformation of the structure around the impurity is needed. Second Al is more strongly bound in Al_2O_3 than Ga in Ga_2O_3. The enthalpies of formation are $\Delta H_f(\text{Al}) = -15.05$ eV/atom and $\Delta H_f(\text{Ga}) = -10.55$ eV/atom (calculated with LDA).

In summary our calculated formation energies agree very well with the results of other groups although a comparison is difficult due to the different correction schemes and chemical references chosen. An excellent analysis of the origin of the varying results for the case of the oxygen vacancy in ZnO is given by Lany and Zunger.[60]

IV. ELECTRONIC-STRUCTURE RESULTS AND DISCUSSION

A. Bulk band structure of ZnO: LDA vs SIC-LDA

In Fig. 6 our LDA result for the band structure of bulk ZnO in the wurtzite structure is shown. Each group of bands is labeled according to the dominant orbitals involved. Our result agrees with previously reported LDA band structures of ZnO.[52,62,63] With respect to experimental results the 3*d* bands are about 2.5 eV too close to the O 2*p* bands. In

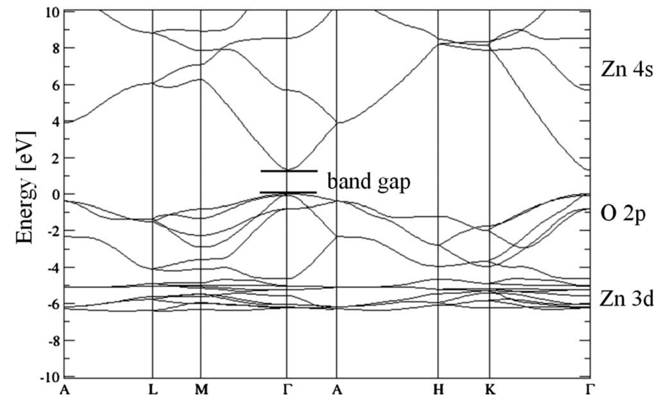

FIG. 6. Band structure of bulk ZnO (in the wurtzite structure) calculated in LDA. The valence-band maximum (VBM) is set to 0 eV. We find a LDA band gap of 1.13 eV. The primary orbital character for each group of bands is indicated on the right-hand side.

experiment[71] the average *d*-band energy is at −7.8 eV relative to the valence band edge. Furthermore the LDA band gap of only 1.13 eV is much smaller than the experimental gap of 3.4 eV.[69] Figure 7 shows our result with the SIC-PP LDA approach. Again this agrees well with the previously published SIC-LDA results.[52,62,63] For the Zn atoms we only applied the SIC to the almost occupied 3*d* orbitals ($w_2=1$) and left the 4*s* and 4*p* orbitals uncorrected as these are almost unoccupied in ZnO. In the case of O we fully corrected the 2*s* orbitals ($w_0=1$) but only partially corrected the 2*p* orbital ($w_1=0.8$) as their average occupation is about 0.8. A value of $\alpha=0.8$ led to a very satisfying band gap of 3.39 eV. The largest effect of the SIC is the downshift of the *d* bands which are then well separated from the O 2*p* bands. Our calculated O 2*p* valence band width of 4.8 eV is slightly less than the measured bandwidth of 5.3 eV.[71] Only the width of 3*d* bands which should be about 2.5 eV remains underestimated by about 1 eV. This is however of minor importance as for the dopants we are interested in the energy region around band gap.

In summary, with the choice of SIC parameters given above in Table I our calculated band structure is remarkably

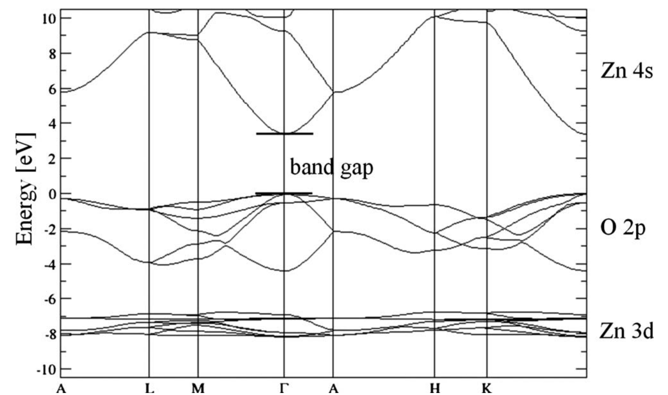

FIG. 7. Band structure of bulk ZnO (in the wurtzite structure) calculated with modified SIC PP. The VBM is set to 0 eV. Again each group of bands is labeled according to the dominant orbitals involved. With respect to LDA, the band gap is increased to 3.39 eV and the *d*-band center shifted down to 7.5 eV.

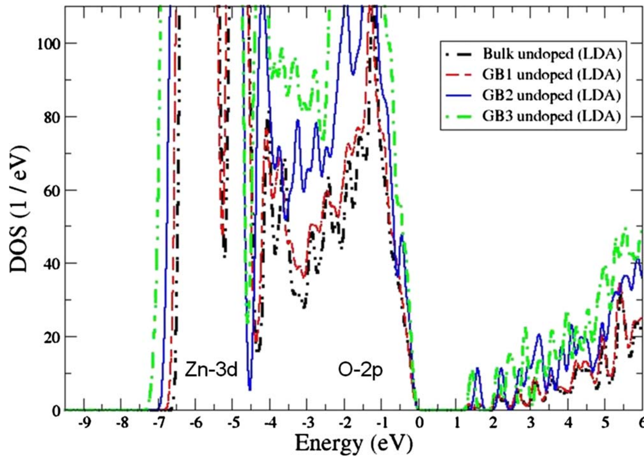

FIG. 8. (Color online) Comparison of the total densities of states of the three grain boundaries and the perfect wurtzite crystal calculated with LDA. All systems show the same (small) band gap and too high Zn 3*d* bands. The zero of energy marks the highest occupied state.

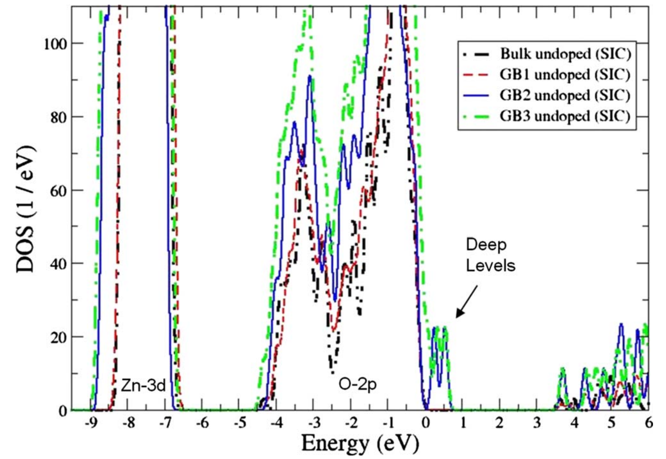

FIG. 9. (Color online) Comparison of the total densities of states for the three grain boundaries and the perfect wurtzite crystal calculated with the SIC-PP scheme. GB1 shows a band gap of about 3.4 eV like the bulk structure. GB2 and GB3 have deep lying electronic gap states above VBM which do not appear in the corresponding LDA calculation (see Fig. 8). The deep levels are occupied in the neutral supercell.

close to the experimentally observed band structure of ZnO. In the following we use these SIC PPs in order to determine the distribution of defect levels in doped grain-boundary and single crystal supercells.

B. Electronic defect levels at GB in pure ZnO

The main focus of this work is to investigate additional energy levels created by the dopants in the energy gap of ZnO in order to get an assessment of the different dopants with respect to optical transparency and electrical conductivity. First, we present our results for the three GBs in the undoped ZnO. We use as starting point the SIC PP for Zn and O which reproduce very well the band structure of perfect wurtzite crystal (see Fig. 7). Of course, there are redistributions of electrons due to grain boundaries or dopants which might influence the occupation of certain Zn or O orbitals. However, such local changes in occupation are likely small (order of few percent) and therefore neglected.

In Fig. 8 sections of the total electronic densities of states (DOSs) for the three GBs and the perfect wurtzite crystal calculated with LDA are depicted. Besides the too high 3*d* bands and the too small band gap one notices that the DOSs of the GB only slightly deviate from the DOSs of the perfect crystal. Differences in absolute value of the DOS are due to the different numbers of atoms in the supercells. Performing similar calculations several groups concluded that undoped GBs do not create deep states.[33–40] Our results of SIC-PP calculations contradict this earlier conclusion. In Fig. 9 the total DOSs for the bulk and the GB evaluated with the SIC PP are shown. GB2 and GB3 have deep levels above the VBM. Also at the upper edge of the band gap additional levels appear. A closer analysis of these levels showed that the levels originate from oxygen atoms located directly at the boundaries. These oxygen atoms have dangling 2*p* bonds. This is the decisive structural difference of GB2 and GB3 from GB1 where every oxygen atom is surrounded by four zinc atoms resulting in lower 2*p* orbitals.

In the course of our work it turned out that our four considered host systems (bulk crystal and three GBs) could be divided into two pairs. On the one hand the dopants influenced the level structure similarly in the bulk and GB1. On the other hand the defects showed similar behavior in GB2 and GB3. Therefore we present in the following only results of the bulk crystal and GB2 in order to simplify the presentation with respect to the number of displayed curves per figure.

The oxygen vacancy is an intrinsic defect in ZnO that has been extensively studied before. Several experiments have attributed the green luminescence seen in ZnO (emission energy of 2.4 eV) to oxygen vacancies. Zhang *et al.*[4] compared the energy levels predicted by different methods. Sophisti-

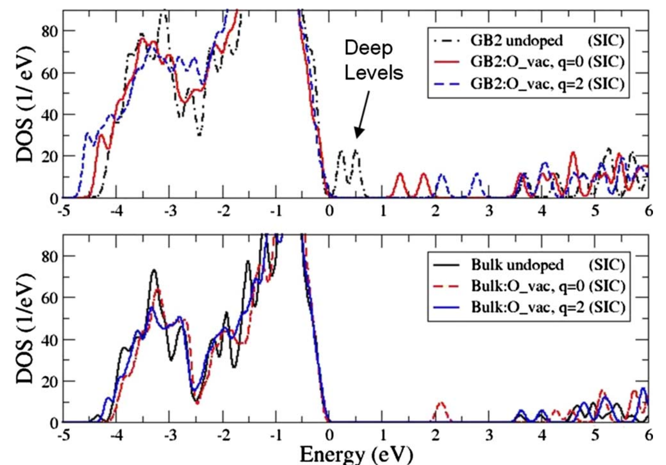

FIG. 10. (Color online) The total density of states of GB2 and the bulk crystal with an oxygen vacancy. In the bulk crystal the neutral charge state of the oxygen vacancy lies at about 2.2 eV above the VBM which makes it a possible source for the green luminescence of ZnO.

cated electronic-structure models such as SIC[52] or *GW* [72] predict a deep level lying about 1 eV below the CBM. Our SIC findings for the bulk crystal depicted in the lower panel of Fig. 10 agree rather well with these predictions. The center of the additional oxygen vacancy level ($q=0$) is 2.2 eV above the VBM or 1.2 eV below the CBM. It is generally believed[4] that the *n* conductivity of undoped ZnO can be attributed to the doubly positive charged oxygen vacancy since it creates additional levels around the conduction band. For the bulk crystal and GB2 our calculations predict additional levels due to the oxygen vacancy in the conduction band (for both charge states). Furthermore the deep levels above the VBM originating from the oxygen atoms right at GB2 that have dangling bonds disappear. The oxygen vacancy provides space for a better accommodation of the oxygen atoms at the boundary.

C. Electronic defect levels at GB in doped ZnO

Next we discuss the influence of the various dopants on the total density of states. Notice that for N, P, Al, and Ga in ZnO there is no such obvious bulk reference host like ZnO itself for Zn and O which allows us to adjust the SIC-PP modeling. As already mentioned above the defect occupation may vary depending on the location in the ZnO material. Hence a unique first-principles way of modeling the impurity SIC PP is not fully achieved yet. As a physical guideline one should choose the weight factors w_l according to the orbital occupation like we did in the case of Zn and O. One might expect, for example, that due to the smaller electronegativity of nitrogen that the nitrogen 2*p* orbitals are less occupied than the oxygen 2*p* orbitals which should result in a smaller weight factor w_1. As the occupation varies only weakly for our dopants we choose the weight factors of them according to the atom they substitute (see Table I). For nitrogen, for example, it is $w_1=0.8$ like for oxygen.

1. *p-type dopants N and P in ZnO*

According to Fig. 4 N_O is the decisive defect state. Other charge states such as N_O^- or N_O^{2-} are less favorable. Theoretical studies[6,9] using bulk supercells indicate that the acceptor level of N is so deep that it is difficult to explain *p* conductivity at room temperature by such defects. Our SIC-PP calculation of total DOS depicted in Fig. 11 confirms deep levels for the bulk. However, the picture changes when a nitrogen impurity is situated at the GB2 (see upper panel of Fig. 11). A continuum of additional levels above the valence band edge appears. The interaction of the GB with the nitrogen impurity leads shallow levels which thus allow us to explain the *p* conductivity due to nitrogen doping.

A similar picture is obtained by looking at the total DOS of the P-doped system. Our SIC-PP calculation predicts a deep level in the band gap of the single crystal (see lower panel of Fig. 12). Again the distribution of levels is changed in the presence of the GB2 grain boundary where the interaction of the impurity with GB2 leads to shallow levels above the VBM thus enabling electrical (semi)conduction at room temperature. Increasing the impurity concentration for substitutional N_O and P_O dopings may considerably decrease

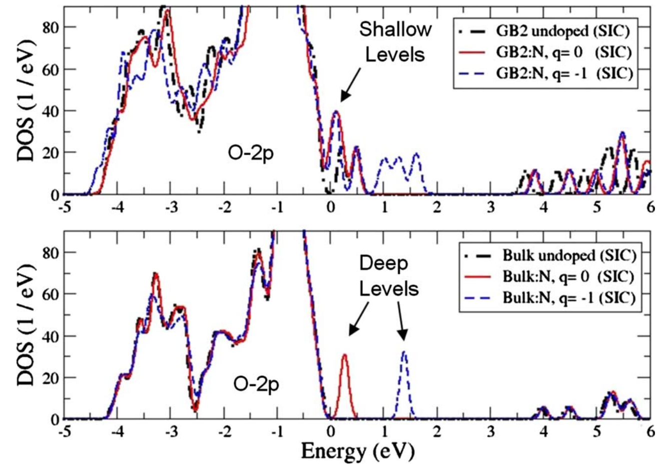

FIG. 11. (Color online) The total densities of states of the N-doped GB2 and the bulk crystal. The N_O and N_O^- impurities in the bulk crystal generate isolated deep levels. However, positioned at GB2 N_O and N_O^- create shallow levels above the VBM which might provide an explanation for the origin of *p* conductivity due to N doping at room temperature.

the optical transparency since the gap is getting closed by additional levels.

2. *n-type dopants Al and Ga in ZnO*

The modifications of the total density of states due to substitutional Al_{Zn} or Ga_{Zn} doping are not that clearly visible as above for the anion dopants. In Fig. 13 one can see that the neutral and the positively charged Al dopants create additional levels in the conduction band of the host. Furthermore one observes that the deep levels above the VBM originating from the oxygen atoms right at GB2, which have

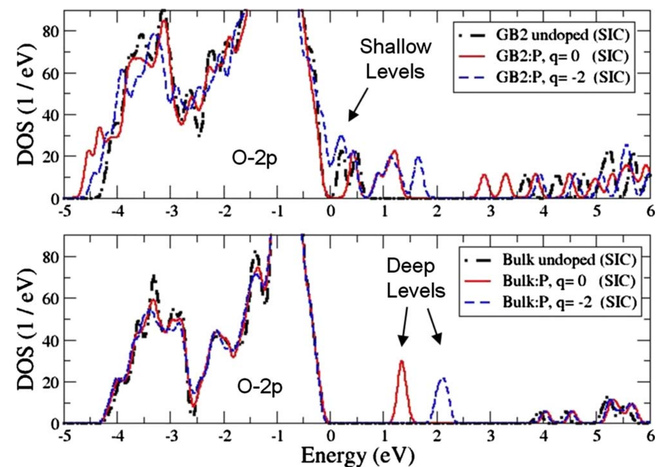

FIG. 12. (Color online) The total densities of states of the P-doped GB2 and the bulk crystal. The P_O and P_O^{2-} impurities generate isolated deep levels in the band gap of the bulk crystal. However, positioned at GB2 P_O and P_O^{2-} create shallow levels above the VBM. Also below the conduction band additional states appear. For high doping concentrations a reduction of the optical transparency can be expected. (The other charge states $P_O^-, P_O^{3-}, \ldots$ are found to be almost identical to the P_O^{2-} states.)

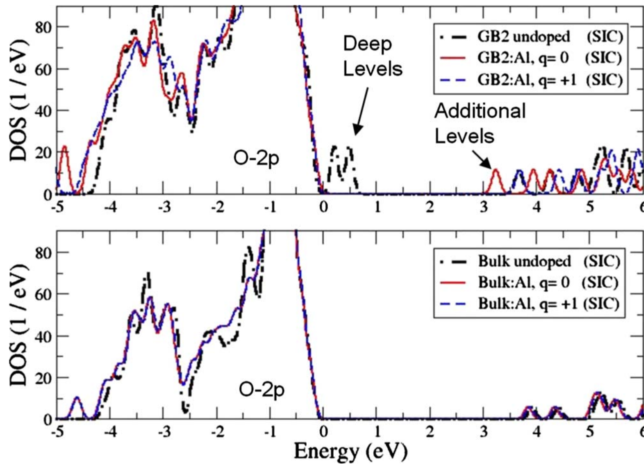

FIG. 13. (Color online) The total densities of states of the Al-doped GB2 and bulk crystal. The Al_{Zn} and ${Al_{Zn}}^{+}$ generate additional levels in the conduction band of the bulk. In the GB2 Al_{Zn} and ${Al_{Zn}}^{+}$ create shallow donor levels and make the deep acceptor levels stemming from the GB2 disappear completely.

dangling bonds, disappear (i.e., the band gap reopens). This happens because a smaller aluminum atom substituting a larger zinc atom provides space for a better accommodation of the oxygen atoms at the boundary. Thus Al doping of crystalline ZnO can even increase the transparency of the material for wavelength λ larger than 380 nm. This effect has been reported by Park *et al.* (see Fig. 6 in Ref. 73) and by Papadopoulou *et al.* (see Fig. 2 in Ref. 74). Both groups observed an increase of the optical transparency of several percent for $\lambda > 380$ nm if they dope pure polycrystalline ZnO with Al. This may be explained by the mechanism described above.

For Ga doping as well we see a reduction of the deep levels above the VBM of GB2 (see Fig. 14). However, compared to Al doping the effect is reduced. The gallium atoms are more similar in size to zinc atoms, therefore offer less space at the grain boundary, and thus inhibit partially the accommodation of the oxygen atoms. Also such an increase of transparency that we predict from our DOS analysis is seen in experiment by Park *et al.*[73] They found an increase of transparency of several percent for polycrystalline ZnO:Ga as compared to the undoped ZnO. Concerning the electronic conductivity, Ga doping, like Al-doping as well, leads to additional states near the conduction band of ZnO. The good *n*-type conductivity that one can expect from these donor states is seen also experimentally.[73,74]

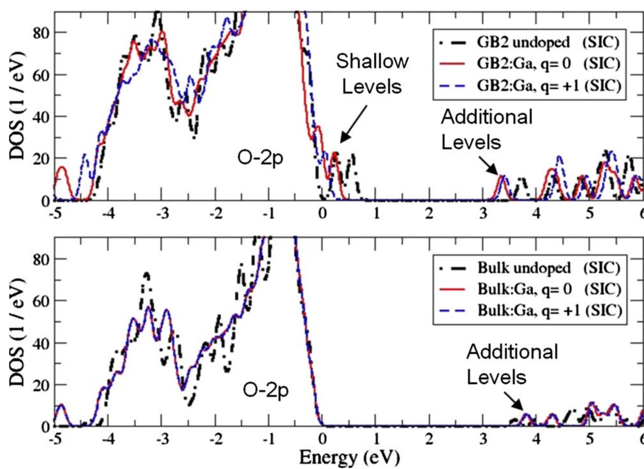

FIG. 14. (Color online) The total densities of states of the Ga-doped GB2 and bulk crystal. The Ga_{Zn} and ${Ga_{Zn}}^{+}$ generate additional levels in the conduction band of the bulk. In the GB2 Ga_{Zn} and ${Ga_{Zn}}^{+}$ not only create shallow donor levels but also make the deep acceptor levels coming from oxygen atoms with dangling bonds disappear partially.

V. SUMMARY AND CONCLUSIONS

In summary, a comparative study of dopant elements at different grain boundaries and in the bulk single crystal of ZnO with the wurtzite structure was carried out. We showed that taking into account the grain boundaries in ZnO is crucial for the analysis and understanding of certain electronic effects of dopants. The picture that emerges from our first-principles DFT supercell calculations, answering the three principal questions posed in Sec. I, can be summed up as follows:

(1) We see a trend of segregation to the grain boundaries for phosphorus. This trend to segregate can be rationalized by the size mismatch of the substitutional dopant and the substituted oxygen host atom.

(2) Our LDA analysis of the defect-formation energies as a function of charge states and chemical potentials agreed mostly with the earlier findings in the literature for the bulk structure. The defect-formation energies for the dopants at the grain boundaries can differ by several eV from the perfect crystal values. Nevertheless we do not identify any change in the hierarchy of elements. N is a more favorable candidate than P in all bulk and boundary structures. Similarly Ga has a lower defect-formation energy than Al. The hierarchy of the different charge states is preserved in the GB and bulk supercells.

The total densities of states determined with our SIC-PP approach show a number of interesting and important results:

(3) According to our SIC-LDA calculations stoichiometric and undoped grain boundaries can create deep lying defect levels (see Fig. 9). This finding is different from our own LDA results (see Fig. 8) and those reported earlier in the literature.[33–35,39] The reason why LDA produces strongly deviating results most likely lies in the much to high $3d$ bands of Zn, which lead to their unrealistic interaction with the O $2p$ bands, shifting these too high in energy. That prevents the appearance of the deep defect states in the band gap.

(4) All dopants create modified defect levels near grain boundaries. They tend to be smeared out but also their positions can change.

(4.1) The position of the additional levels generated by oxygen vacancies as found by SIC PP can explain the behavior of oxygen vacancies as an intrinsic source of n conductivity as well as being responsible for the green luminescence that is observed (see Fig. 10).

(4.2) The problem of how to explain p conductivity by N doping can be solved with the help of grain boundaries. The

deep levels due to N doping that appear in the bulk structure are strongly modified near certain grain boundaries and lead to shallow levels above the VBM. A similar behavior is observed for P. For both N and P dopings we expect a decrease of the optical transparency for high doping concentrations since we found numerous additional levels filling the band gap (see Figs. 11 and 12).

(4.3) From our presented graphs for the total densities of states of Al- and Ga-doped systems one can understand that the two dopants enhance the *n* conductivity. In the case of Al and Ga we do not find any closing of the energy gap by deep levels of the dopants, so that a good transparency is expected even for high dopant concentrations. For polycrystalline ZnO samples, Al and Ga dopings suppress deep levels originating from oxygen atoms with dangling bonds (see Figs 13 and 14) which might explain the experimentally observed increase of transparency for wavelength $\lambda > 380$ nm.[73,74]

This theoretical atomic-scale electronic-structure study, although confined to only four substitutional dopants and three GB models, demonstrated the importance of internal boundaries for functional (electronic, optical, and electric) properties of doped TCO materials. This was not yet fully recognized so far and likely will become a relevant aspect in the search for TCO materials with improved transparency and conductivity. Furthermore the work illustrated that the combination of first-principles LDA and SIC-PP calculations is powerful and applicable to extended atomistic defect structures.

ACKNOWLEDGMENTS

Financial support for the work was provided by the Fraunhofer-Gesellschaft in Germany (MAVO project METCO). We acknowledge many discussions with the project partners B. Szyszka (Fraunhofer IST), P. Loebmann (Fraunhofer ISC), A. Georg, D. Borchert (Fraunhofer ISE), and C. May (Fraunhofer IPMS), and we thank N. Schulz (Schott) and T. Brammer (Q-Cells) for their valuable comments.

*wolfgang.koerner@iwm.fraunhofer.de

[1] P. Erhart and K. Albe, Phys. Rev. B **73**, 115207 (2006).
[2] P. Erhart, K. Albe, and A. Klein, Phys. Rev. B **73**, 205203 (2006).
[3] A. F. Kohan, G. Ceder, D. Morgan, and Chris G. Van de Walle, Phys. Rev. B **61**, 15019 (2000).
[4] S. B. Zhang, S. H. Wei, and A. Zunger, Phys. Rev. B **63**, 075205 (2001).
[5] J. L. Zhao, W. Zhang, X. M. Li, J. W. Feng, and X. Shi, J. Phys.: Condens. Matter **18**, 1495 (2006).
[6] E.-C. Lee, Y.-S. Kim, Y.-G. Jin, and K. J. Chang, Phys. Rev. B **64**, 085120 (2001).
[7] E. C. Lee and K. J. Chang, Phys. Rev. B **70**, 115210 (2004).
[8] W. J. Lee, J. Kang, and K. J. Chang, Phys. Rev. B **73**, 024117 (2006).
[9] C. H. Park, S. B. Zhang, and S. H. Wei, Phys. Rev. B **66**, 073202 (2002).
[10] S. Limpijumnong, S. B. Zhang, S.-H. Wei, and C. H. Park, Phys. Rev. Lett. **92**, 155504 (2004).
[11] Y. Yan and S.-H. Wei, Phys. Status Solidi B **245**, 641 (2008).
[12] L. G. Wang and A. Zunger, Phys. Rev. Lett. **90**, 256401 (2003).
[13] Y. Yan, J. Li, S.-H. Wei, and M. M. Al-Jassim, Phys. Rev. Lett. **98**, 135506 (2007).
[14] F. Oba, H. Ohta, Y. Sato, H. Hosono, T. Yamamoto, and Y. Ikuhara, Phys. Rev. B **70**, 125415 (2004).
[15] K. L. Merkle and D. J. Smith, Phys. Rev. Lett. **59**, 2887 (1987).
[16] U. Dahmen, S. Paciornik, I. G. Solorzano, and J. B. Vanderzande, Interface Sci. **2**, 125 (1994).
[17] S. Fabris and C. Elsässer, Phys. Rev. B **64**, 245117 (2001).
[18] S. Fabris and C. Elsässer, Acta Mater. **51**, 71 (2003).
[19] C. Elsässer and A. E. Marinopolous, Acta Mater. **49**, 2951 (2001).
[20] H. Nishimura, K. Matsunaga, T. Saito, T. Yamamoto, and Y. Ikuhara, J. Am. Ceram. Soc. **86**, 574 (2003).
[21] K. Matsunaga, H. Nishimura, T. Saito, T. Yamamoto, and Y. Ikuhara, Philos. Mag. **83**, 4071 (2003).
[22] S. Nufer, A. G. Marinopoulos, T. Gemming, C. Elsässer, W. Kurtz, S. Köstlmeier, and M. Rühle, Phys. Rev. Lett. **86**, 5066 (2001).
[23] V. Ravikumar, V. P. Dravid, and D. Wolf, Interface Sci. **8**, 157 (2000).
[24] Z. Zhang, W. Sigle, F. Philipp, and M. Rühle, Science **302**, 846 (2003).
[25] M. M. McGibbon, N. D. Browning, M. F. Chisholm, A. J. McGibbon, S. J. Pennycook, V. Ravikumar, and V. P. Dravid, Science **266**, 102 (1994).
[26] N. Shibata, F. Oba, T. Yamamoto, and Y. Ikuhara, Philos. Mag. **84**, 2381 (2004).
[27] V. Potin, P. Ruterana, G. Nouet, R. C. Pond, and H. Morkoc, Phys. Rev. B **61**, 5587 (2000).
[28] A. Béré and A. Serra, Philos. Mag. **86**, 2159 (2006).
[29] C. Elsässer and T. Elsässer, J. Am. Ceram. Soc. **88**, 1 (2005).
[30] N. A. Benedek, Alvin L.-S. Chua, C. Elsässer, A. P. Sutton, and M. W. Finnis, Phys. Rev. B **78**, 064110 (2008).
[31] Y. Sato and T. Yamamoto, J. Am. Ceram. Soc. **90**, 337 (2007).
[32] P. Ruterana, M. Abouzaid, A. Bere, and J. Chen, J. Appl. Phys. **103**, 033501 (2008).
[33] F. Oba, I. Tanaka, S. R. Nishitani, H. Adachi, B. Slater, and D. H. Gay, Philos. Mag. A **80**, 1567 (2000).
[34] F. Oba, H. Adachi, and I. Tanaka, J. Mater. Res. **15**, 2167 (2000).
[35] F. Oba, S. R. Nishitani, H. Adachi, I. Tanaka, M. Kohyama, and S. Tanaka SWING, Phys. Rev. B **63**, 045410 (2001).
[36] H. S. Domingos, J. M. Carlsson, P. D. Bristowe, and B. Hellsing, J. Phys.: Condens. Matter **14**, 12717 (2002).
[37] J. M. Carlsson, H. S. Domingos, B. Hellsing, and P. D. Bristowe, Interface Sci. **9**, 143 (2001).
[38] J. M. Carlsson, B. Hellsing, H. S. Domingos, and P. D. Bristowe, Surf. Sci. **532-535**, 351 (2003).
[39] J. M. Carlsson, H. S. Domingos, P. D. Bristowe, and B. Hellsing, Phys. Rev. Lett. **91**, 165506 (2003).

[40] J. M. Carlsson, B. Hellsing, H. S. Domingos, and P. D. Bristowe, J. Phys.: Condens. Matter **13**, 9937 (2001).
[41] S. H. Wei and A. Zunger, Phys. Rev. B **37**, 8958 (1988).
[42] J. L. Martins, N. Troullier, and S. H. Wei, Phys. Rev. B **43**, 2213 (1991).
[43] P. Schröer, P. Krüger, and J. Pollmann, Phys. Rev. B **47**, 6971 (1993).
[44] P. Schröer, P. Krüger, and J. Pollmann, Phys. Rev. B **48**, 18264 (1993).
[45] S. B. Zhang, S. H. Wei, and A. Zunger, Phys. Rev. B **52**, 13975 (1995).
[46] L. Ley, R. A. Pollak, F. R. McFelly, S. P. Kowalczyk, and D. Shirley, Phys. Rev. B **9**, 600 (1974).
[47] H. Lüth, G. W. Rubloff, and W. D. Grobman, Solid State Commun. **18**, 1427 (1976).
[48] W. Ranke, Solid State Commun. **19**, 685 (1976).
[49] G. Zwicker and K. Jacoby, Solid State Commun. **54**, 701 (1985).
[50] R. Weidemann, H. E. Gumlich, M. Kupsch, H. U. Middelmann, and U. Becker, Phys. Rev. B **45**, 1172 (1992).
[51] J. P. Perdew and A. Zunger, Phys. Rev. B **23**, 5048 (1981).
[52] D. Vogel, P. Krüger, and J. Pollmann, Phys. Rev. B **54**, 5495 (1996).
[53] C. Elsässer, N. Takeuchi, K. M. Ho, C. T. Chan, P. Braun, and M. Fähnle, J. Phys.: Condens. Matter **2**, 4371 (1990).
[54] K. M. Ho, C. Elsässer, C. T. Chan, and M. Fähnle, J. Phys.: Condens. Matter **4**, 5189 (1992).
[55] B. Meyer, C. Elsässer, and M. Fähnle, FORTRAN 90 program for mixed-basis pseudopotential calculations for crystals, Max-Planck Institut für Metallforschung, Stuttgart.
[56] B. Meyer, K. Hummler, C. Elsässer, and M. Fähnle, J. Phys.: Condens. Matter **7**, 9201 (1995).
[57] F. Lechermann, M. Fähnle, B. Meyer, and C. Elsässer, Phys. Rev. B **69**, 165116 (2004).
[58] D. M. Ceperley and B. J. Alder, Phys. Rev. Lett. **45**, 566 (1980).
[59] D. Vanderbilt, Phys. Rev. B **32**, 8412 (1985).
[60] S. Lany and A. Zunger, Phys. Rev. B **78**, 235104 (2008).
[61] C. Persson, Y. J. Zhao, S. Lany, and A. Zunger, Phys. Rev. B **72**, 035211 (2005).
[62] A. Filippetti and N. A. Spaldin, Phys. Rev. B **67**, 125109 (2003).
[63] C. D. Pemmaraju, T. Archer, D. Sanchez-Portal, and S. Sanvito, Phys. Rev. B **75**, 045101 (2007).
[64] F. Decremps, F. Datchi, A. M. Saitta, A. Polian, S. Pascarelli, A. Di Cicco, J. P. Itie, and F. Baudelet, Phys. Rev. B **68**, 104101 (2003).
[65] W. H. Press, B. P. Flannery, S. A. Teukolsky, and W. T. Vettering, *Numerical Recipies* (Cambridge University Press, Cambridge, 1986), Chap. 10.7.
[66] C. G. Van de Walle and J. Neugebauer, J. Appl. Phys. **95**, 3851 (2004).
[67] Y. Yan, S. B. Zhang, and S. T. Pantelides, Phys. Rev. Lett. **86**, 5723 (2001).
[68] *Handbook of Chemistry and Physics*, 73 ed., edited by D. R. Lide (CRC, Boca Raton, FL, 1992).
[69] M. Oshikiri and F. Aryasetiawan, Phys. Rev. B **60**, 10754 (1999).
[70] S. Lany and A. Zunger, Phys. Rev. Lett. **98**, 045501 (2007).
[71] *Semiconductors Physics of Group 4 Elements and 3-5 Compounds*, edited by K. H. Hellwege and O. Madelung, Landolt-Börnstein, New Series, Group 3, Vol. 17, Pt. A (Springer, Berlin, 1982); *Semiconductors: Intrinsic Properties of Group 4 Elements and 3-5-7, and 1-7 Compounds*, edited by K. H. Hellwege and O. Madelung, Landolt-Börnstein, New Series, Group 3, Vol. 22, Pt. A (Springer, Berlin, 1987).
[72] P. A. Sterne and J. C. Inkson, J. Phys. C **17**, 1497 (1984).
[73] S.-M. Park, T. Ikegami, K. Ebihara, and P.-K. Shin, Appl. Surf. Sci. **253**, 1522 (2006).
[74] E. L. Papadopoulou, M. Varda, K. Kouroupis-Agalou, M. Androulidaki, E. Chikoidze, P. Galtier, G. Huyberechts, and E. Aperathitis, Thin Solid Films **516**, 8141 (2008).